Astronomy & Astrophysics manuscript no. master
March 1, 2017

High resolution near-IR spectroscopy of Arcturus and 10 Leo

Refining a near-IR iron line list

D. T. Andreasen[1,2], S. G. Sousa[1], E. Delgado Mena[1], N. C. Santos[1,2], T. Lebzelter[3], and A. Mucciarelli[4,5]

[1] Instituto de Astrofísica e Ciências do Espaço, Universidade do Porto, CAUP, Rua das Estrelas, 4150-762 Porto, Portugal, e-mail: daniel.andreasen@astro.up.pt
[2] Departamento de Física e Astronomia, Faculdade de Ciências, Universidade do Porto, Rua Campo Alegre, 4169-007 Porto, Portugal
[3] Institute for Astrophysics, University of Vienna, Türkenschanzstrasse 17, 1180 Vienna, Austria
[4] Dipartimento di Fisica e Astronomia, Universita' degli Studi di Bologna, Viale Berti Pichat, 6/2, 40126, Bologna, Italy
[5] INAF - Osservatorio Astronomico di Bologna, Via Ranzani 1, 40127, Bologna, Italy

Received ...; accepted ...

ABSTRACT

Context. Effective temperature, surface gravity, and metallicity are basic spectroscopic stellar parameters necessary to characterise a star or a planetary system. Reliable atmospheric parameters for FGK stars have been obtained mostly from methods that rely on high resolution and high signal-to-noise optical spectroscopy. The advent of a new generation of high resolution near-IR spectrographs opens the possibility of using classic spectroscopic methods with high resolution and high signal-to-noise in the NIR spectral window.
Aims. We aim to obtain precise and accurate atmospheric stellar parameters using high quality spectra of two early type K giant stars.
Methods. Our spectroscopic analysis is based on the iron excitation and ionization balance done in LTE and a line list Fe I and Fe II lines in the NIR domain.
Results. We get good results!

Key words. data reduction: high resolution spectra – stars individual: Arcturus – stars individual: 10 Leo

1. Introduction

Effective temperature ($T_{\rm eff}$), surface gravity ($\log g$), and metallicity ([M/H], where iron is normally used as a proxy) are fundamental atmospheric parameters necessary to characterise a single star, and to determine other indirectly fundamental parameters such as mass, radius, and age from stellar evolution models (see e.g. Girardi et al. 2000; Dotter et al. 2008; Baraffe et al. 2015). Precise and accurate stellar parameters are also essential in exoplanet searches. Planetary radius and mass are mainly found from transit lightcurve analysis and radial velocity analysis, respectively. The determination of the mass of the planet implies a knowledge of the stellar mass, while the measurement of the radius of the planet is dependent on our capability to derive the radius of the star (see e.g. Torres et al. 2008; Ammler-von Eiff et al. 2009; Torres et al. 2012).

The derivation of precise stellar atmospheric parameters is not a simple task. Different approaches often lead to discrepant results (see e.g. Lebzelter et al. 2012; Santos et al. 2013). Interferometry is usually considered an accurate method for deriving stellar radii (see e.g. Boyajian et al. 2012); however, it is only applicable for bright nearby stars. Asteroseismology, on the other hand, reveals the inner stellar structure by observing the stellar pulsations at the surface. From asteroseismology it is possible to measure the surface gravity and mean density, and therefore to calculate the mass and radius with high precision (e.g. Kjeldsen & Bedding 1995). However, for stars on the main sequence asteroseismic methods can typically only be applied to FG stars, since the oscillation modes of K and M dwarfs are likely too weak to be detected even with high precision spectroscopy or photometry.

A crucial parameter for the indirect determination of stellar bulk properties is the effective temperature. In that respect, the infrared flux method (IRFM) has proven to be reliable for FGK dwarf and subgiant stars. For higher accuracy the IRFM needs a priori knowledge of the bolometric flux, reddening, surface gravity, and stellar metallicity (Blackwell & Shallis 1977; Ramírez & Meléndez 2005; Casagrande et al. 2010).

Finally, the use of high resolution spectroscopy along with stellar atmospheric models is an extensively tested method that allows the derivation of the fundamental parameters of a star (see e.g. Valenti & Fischer 2005; Santos et al. 2013). The procedure depends on the quality of the spectra, their resolution, and wavelength region. A fit to the overall spectrum can be applied for all spectral resolutions, but are often time consuming (see e.g. Recio-Blanco et al. 2006). For resolutions higher than $\lambda/\Delta\lambda < 20\,000$ we can apply the equivalent width (EW) method (see e.g. Tsantaki et al. 2013; Andreasen et al. 2017, for details). However, while the latter approach is often faster than the synthetic fitting, it requires higher quality spectra, and the star to be a slow rotating (below 10 km/s to 15 km/s).

Standard procedures are often used to derive stellar atmospheric parameters from high quality spectra in the optical (see e.g. Valenti & Fischer 2005; Sousa et al. 2008). With the advancement of high resolution near-infrared (NIR) instruments, we will now be able to use a similar technique to that used in the optical part of the spectrum (see e.g. Meléndez & Barbuy 1999; Sousa et al. 2008; Tsantaki et al. 2013; Mucciarelli et al. 2013; Bensby et al. 2014). At the moment, the GIANO spec-

trograph installed at *Telescopio Nazionale Galileo* (TNG) is already available (Origlia et al. 2014), as is the *infrared Doppler instrument* (IRD) installed at the Subaru telescope (Kotani et al. 2014), *Calar Alto high-Resolution search for M dwarfs with Exoearths with Near-infrared and optical Échelle Spectrographs* (CARMENES) for the 3.5 m telescope at Calar Alto Observatory (Quirrenbach et al. 2014), and iShell at the *InfraRed Telescope Facility* (Rayner et al. 2012, 2016). Three new spectrographs are planned for the near future: 1) The *CRyogenic InfraRed Echelle Spectrograph Upgrade Project* (CRIRES+) at the *Very Large Telescope* (VLT) (Follert et al. 2014) with expected first light in 2017, 2) *un SpectroPolarimètre Infra-Rouge A Near-InfraRed Spectropolarimeter* (SPIRou) at *The Canada-France-Hawaii Telescope* (CFHT) (Delfosse et al. 2013; Artigau et al. 2014) with expected first light in 2017 as well, and 3) NIRPS at the ESO 3.6m telescope in La Silla (Conod et al. 2016). The spectral resolutions for these spectrographs range between 50 000 and 100 000.

With the advance of the next generation NIR spectrographs, we are still preparing the data analysis of stellar spectra, in particular how to get reliable atmospheric parameters (see e.g. Önehag et al. 2012; Lindgren et al. 2016; Andreasen et al. 2016). The analysis of stellar spectra is well understood for FGK stars in the optical part of the spectrum, however some work still needs to be done for the NIR part.

We continue our series of studies to explore the use of the NIR domain to derive stellar parameters for FGK and M stars. In particular, here we analyse the atlas of Arcturus and the spectrum of 10 Leo. The atlas of Arcturus was acquired at Kitt Peak National Observatory using the FTS spectrograph at the Mayall telescope (Hinkle et al. 2003), meanwhile the spectrum of 10 Leo was taken from CRIRES (Nicholls et al. 2016). For the analysis we use the iron line list presented in Andreasen et al. (2016) (referred to as Paper I). This work is a continuation of our previous work. In Paper I we successfully tested our method on a slightly hotter star than the Sun, while in this work we aim to test the method on cooler stars. The strength of the NIR domain over the optical becomes clear when we move towards the cooler stars. Here we see less continuum depression and line blending due to in particular molecular features. Moreover, the cooler stars emit more light in the NIR domain than the optical, and with the lightest stars being intrinsically faint, we thus obtain the majority of the flux here.

2. Data

While the community is currently on the verge to access large amount of high resolution NIR spectra the available spectra at the moment are sparse. We chose to use two stars cooler than the Sun since we used a hotter star (HD 20010) than the Sun in Paper I. The method used in Paper I and here is determing the iron abundances on a number of lines from their measure EW. Then we impose ionization balance between Fe I and Fe II lines, and excitation balance for all Fe I lines, by changing the atmospheric parameters for the model atmosphere (Kurucz 1993, is used here).

We have used the atlas of Arcturus, one of the brightest stars on the Northern hemisphere. Thus it is well studied (see e.g. Griffin & Griffin 1967; McWilliam 1990; Ramírez et al. 2013, to mention just a few). We use the atlas from Hinkle et al. (2003) which covers the spectral range of interest (YJHK bands). Strong telluric features were identified with a spectrum from the TAPAS web page (Bertaux et al. 2014). The atlas also comes with a telluric standard and the ratio of the two spectra in order to correct for the tellurics. The telluric spectrum from TAPAS is only used for telluric line identification. We use both the telluric corrected and non-corrected.

The second spectrum is from the CRIRES-POP team (Nicholls et al. 2016). 10 Leo is very similar to Arcturus, which is also one reason this star was the first to be fully reduced by the CRIRES-POP team. The spectrum is divided into each band YJ (only together), H, K, L, and M. We use only the first three. Some small gaps are present in the spectrum due to tellurics that could not be properly removed, low S/N, bad pixels, etc. Rather than giving an uncertain interpolation, Nicholls et al. (2016) decided to leave small gaps in the data. This has very little effect on our line by line analysis. However, we were unable to measure one Fe II line due to the gaps, which are generally very important to determine the surface gravity.

The data for the two stars are very similar in terms of S/N (around 300 as measured by IRAF in a continuum region in the YJ band), resolution (approximately 100 000), and spectral coverage. In Fig. 1 we compare the spectra of the two stars in a region with some of the iron lines used for the analysis described below.

3. Refining the NIR line list

Besides testing the line list from Paper I at cooler effective temperatures with two K stars, it is a primary goal of this work to refine the line list. This includes identifying recurring outliers (both from the work done in Paper I and in this work), and lines which we are not able to measure, e.g. if a line is amidst a forest of telluric lines. To identify these lines the solar atlas used in Paper I was revisited. In total 211 Fe I lines and 8 Fe II lines were removed in the process. Most of these were blended lines with either tellurics or other stellar lines. This procedure leaves us with 84 Fe I lines and 5 Fe II lines. These lines should be the best for deploying our technique of determining atmospheric stellar parameters.

During a second look at the Solar spectrum, the EW of the lines were measured by hand (this had been previously done automatically with ARES). Since we re-measured the EWs, the log gf values had to be re-calibrated again. Here we simply change the log gf values for the measured EW until the abundance of a given line is equal to that of the Sun, using the same solar atmosphere model as in Paper I. The mean change in log gf for common lines is -0.09 ± 0.16. The line list with the updated log gf is presented in Appendix A.

The Fe II lines are used to determine $\log g$ by imposing ionization balance with Fe I. However, the low number of Fe II lines available is a concern, since the average abundance of Fe II is affected more by errors, both random and systematic, compared to the Fe I lines. One might fix $\log g$ during the process of obtaining stellar parameters, but this has an impact on the other derived parameters. A more reliable source for $\log g$ could for example be asteroseismology (see e.g. Aerts et al. 2010) or from the parallaxes measured with Gaia (Gaia Collaboration et al. 2016).

4. Results

We derive the stellar atmospheric parameters in the same way as described in Paper I using FASMA (Andreasen et al. 2017). We use ATLAS9 atmosphere models during the derivation (Kurucz 1993). The EWs are measured for both stars automatically with ARES (Sousa et al. 2015) and by hand with splot in IRAF. We compare the derived stellar parameters from the two measured sets of EWs.

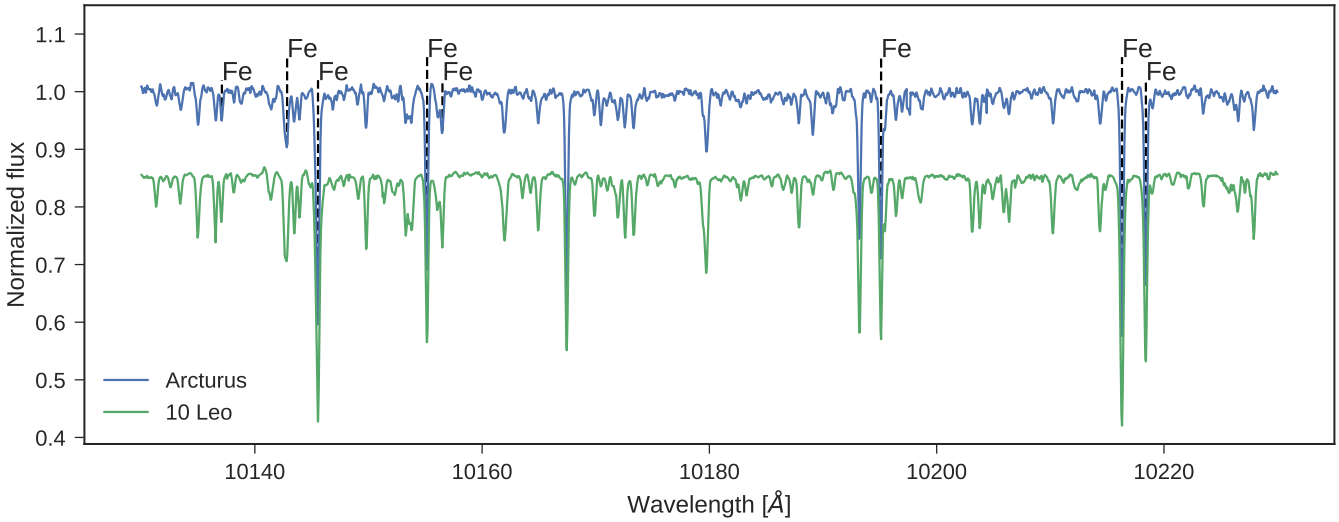

Fig. 1. The spectra of the two stars, in blue is Arcturus, and green is 10 Leo with an 0.15 offset. We mark the location of Fe I lines in the region.

4.1. Revisiting HD 20010

We revisit HD 20010 for which we derived atmospheric stellar parameters in Paper I. This time we remove previously measured lines, which are no longer included in our revised line list. For the rest of the lines the log gf values are updated. The results are presented in Tab. 1 along with the combined literature values (see Paper I and references therein). We see both better agreement with literature values (especially [Fe/H] and log g), and smaller errors with the updated results.

4.2. Arcturus

Arcturus is one of the brightest stars on the night sky with a V magnitude of -0.05 (Ducati 2002). Hence it is a prime target for testing the updated line list with numerous measurements as mentioned above.

The atlas consists of both a summer observation set and a winter observation set. This is in order to minimize the effect of tellurics at different spectral regions. A comparison between the two sets of measured EWs - both the manual measurements using IRAF and the automatic measurements using ARES - are shown in Fig. 2. The automatic EW measurements for the summer set and winter set shows excellent agreement. This means that the two data sets are very similar, thus we chose to only manually measure the EWs for one set (summer). We did, however, measure a few lines from the winter data set to verify the agreement. For both the automatically and manually measured EWs, we discard all lines with an EW below 5 mÅ and above 150 mÅ before continuing the analysis. Lines outside this range are either too weak to be reliable measured or are so strong that the we are not able to fit a Gaussian to the profile. Especially the wings of the absorption lines are a problem for strong lines. For all three sets, parameters were derived with and without log g fixed. The derivation of the parameters follow the procedure presented in Paper I. We use the minimization routine from Andreasen et al. (2017), where one outlier in the abundance is removed iteratively. The final results are presented in Tab. 2 together with mean parameters from the literature.

We generally see good agreement between the derived parameters and the values from the literature. The only parameter

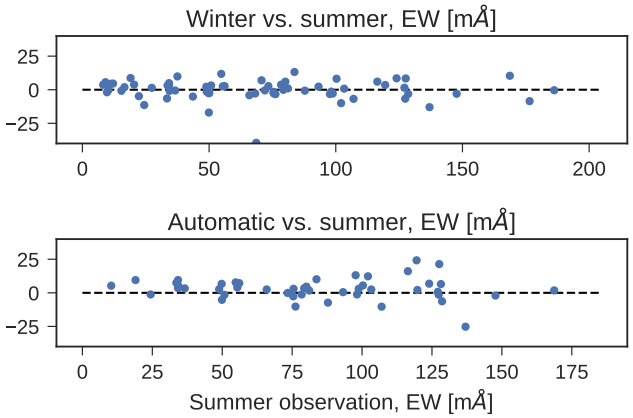

Fig. 2. Top figure: Difference of the automatic EW measurements between the summer observations and winter observations from the Arcturus spectra. Bottom figure: Same as above, but with manual measurements from ARES (summer) and automatic measurements (summer).

being difficult to measure is the surface gravity due to the low number of Fe II lines in the NIR. The metallicity is very important to derive accurately, and we report good results overall, but especially with the automatic measurements, compared to literature values. When measuring this by hand, we might have systematically overestimated the continuum, resulting in higher [Fe/H]. For visualization the parameters are plotted (except $\xi_{\rm micro}$) in Fig. 3. Here the histogram shows the literature values collected from Simbad while the vertical black line is our final value with gray shaded errorbar.

4.3. 10 Leo

The approach for determining the atmospheric stellar parameters for 10 Leo is identical as for Arcturus. The final reduced data is divided in YJ, H, and K bands. We use ARES on each band separately. For the small gaps in the spectrum, we simply set the flux to 1, since the spectrum is already normalized. This will also prevent ARES to measure any lines in these regions. The EWs

Table 1. Updated results for HD 20010 using the shorter line list and new oscillator strengths.

	$T_{\rm eff}$ (K)	$\log g$ (dex)	$\xi_{\rm micro}$ (km/s)	[Fe/H] (dex)
Literature	6131 ± 255	4.01 ± 0.60	1.90 ± 1.08	−0.23 ± 0.14
This work	6157 ± 180	4.06 ± 0.76	1.62 ± 0.44	−0.18 ± 0.11
This work	6153 ± 176	4.01 (fixed)	1.68 ± 0.40	−0.18 ± 0.11
Paper I	6116 ± 224	4.21 ± 0.58	2.45 ± 0.45	−0.14 ± 0.14
Paper I	6144 ± 212	4.01 (fixed)	2.66 ± 0.42	−0.13 ± 0.29

Table 2. The derived parameters for Arcturus with and without fixed surface gravity after 3σ outlier removal. The literature values are a simple mean of all the available parameters on Simbad with the corresponding standard error. There is no microturbulence available, so we derived it using the empirical relation from Adibekyan et al. (2015) for each set of parameters.

	$T_{\rm eff}$ (K)	$\log g$ (dex)	$\xi_{\rm micro}$ (km/s)	[Fe/H] (dex)
Literature	4306 ± 100	1.69 ± 0.32	1.92 ± 0.15	−0.54 ± 0.11
IRAF	4380 ± 79	0.64 ± 0.33	1.14 ± 0.09	−0.49 ± 0.07
IRAF	4212 ± 77	1.69 (fixed)	1.25 ± 0.08	−0.37 ± 0.03
ARES (summer)	4439 ± 63	1.20 ± 0.20	1.55 ± 0.10	−0.58 ± 0.06
ARES (summer)	4348 ± 75	1.69 (fixed)	1.58 ± 0.09	−0.53 ± 0.03
ARES (winter)	4436 ± 67	0.55 ± 1.77	1.35 ± 0.09	−0.56 ± 0.07
ARES (winter)	4233 ± 109	1.69 (fixed)	1.43 ± 0.09	−0.49 ± 0.04
Weighted mean	4421 ± 40	0.96 ± 0.60	1.34 ± 0.05	−0.55 ± 0.04
Weighted mean	4269 ± 51	1.69 (fixed)	1.41 ± 0.05	−0.46 ± 0.02

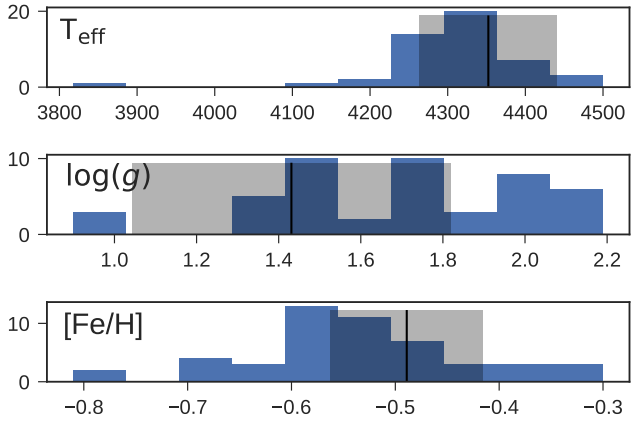

Fig. 3. Histogram of the different sets of literature parameters of Arcturus (except $\xi_{\rm micro}$). The black vertical line are our derived parameters, and the gray shaded area are the errors on the corresponding parameters.

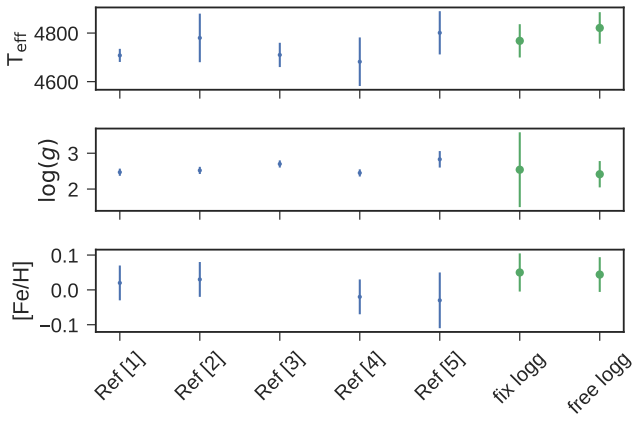

Fig. 4. Literature values (blue) and the two results from this work (green) with and without $\log g$ fixed. The errorbars on the literature values are wither does presented in the corresponding paper, or in the cases none were presented we give an error of 100 K for $T_{\rm eff}$, 0.10 dex for $\log g$, and 0.05 for [Fe/H]. References: Ref [1]: Luck (2015), Ref [2]: Park et al. (2013), Ref [3]: Massarotti et al. (2008), Ref [4]: Soubiran et al. (2008), and Ref [5]: da Silva et al. (2011).

from the three regions are combined to one final line list used for the determination of the parameters. The EWs are also measured by hand using IRAF. We list the result in Tab. 3 alongside with a mean of literature values taken from Simbad. The final results and five collected literature values are presented in Fig. 4.

Generally the derived parameters are in excellent agreement with the literature values listed here. We are able to derive good $\log g$ values, although with larger errors compared to the results from the literature.

5. Discussion

5.1. The role of $\log g$

One of the most difficult atmospheric stellar parameters to get from a spectrum is the surface gravity. Here we need the pressure sensitive ionized atoms such as Fe II. However, they are more sparse than neutral iron, Fe I, making the determination more challenging. This is true in the optical (see e.g. the discussion by Mortier et al. 2013), and even more in the NIR (see e.g. Paper I). One solution to this problem is to fix an estimated value of the surface gravity and derive the other parameters. With the parallaxes from Gaia (Gaia Collaboration et al. 2016) we will have access to accurate $\log g$, thus being able to have good $T_{\rm eff}$ and [Fe/H]. Without the final parallaxes from Gaia we may yet only rely on literature values for $\log g$. As seen from Fig. 3, the distribution of $\log g$ values from the literature are rather disperse. Since there is still a dependence of the other parameters with $\log g$, simply using a mean value as a reference value, can lead to different parameters. This is most likely the cause of the small discrepancies seen for the parameters of Arcturus when the $\log g$

Table 3. Results from 10 Leo presented in the same way as for Tab. 2.

	$T_{\rm eff}$ (K)	$\log g$ (dex)	$\xi_{\rm micro}$ (km/s)	[Fe/H] (dex)
Literature	4720 ± 42	2.54 ± 0.11	1.59 ± 0.02	0.00 ± 0.03
IRAF	4835 ± 85	2.41 ± 0.41	1.28 ± 0.08	0.09 ± 0.06
IRAF	4768 ± 88	2.54 (fixed)	1.20 ± 0.08	0.01 ± 0.05
ARES	4805 ± 98	2.42 ± 0.61	1.23 ± 0.10	−0.01 ± 0.07
ARES	4768 ± 105	2.54 (fixed)	1.20 ± 0.10	−0.01 ± 0.06
Weighted mean	4821 ± 65	2.41 ± 0.37	1.26 ± 0.06	0.04 ± 0.05
Weighted mean	4768 ± 69	2.54 (fixed)	1.20 ± 0.06	0.05 ± 0.04

is fixed and free. With this in mind, the derived parameters are roughly within the errorbars.

To add to the problem of low number of ionized iron lines is the fact that these lines are rather weak. Note that the lowest measured EW for an Fe II line is 7.8 mÅ for Arcturus, while the highest measure value is 20.7 mÅ (measured in 10 Leo). This means that the error on these EWs are relatively high, and become even more problematic for lower S/N spectra. However, with the upcoming high quality spectra for the NIR, the community should still be able to see these Fe II lines.

5.2. Proper data reduction

In our previous work we had problems getting reliable atmospheric stellar parameters for HD 20010. This was partially due to the unfinished data reduction of from CRIRES-POP used at the time. Here the wavelength calibration was done automatically and therefore not optimal. This meant the wavelength was stretched when compared to a synthetic spectrum, which is discussed in more detail by Nicholls et al. (2016). The poor wavelength calibration for HD 20010 most likely caused bad EW measurements. In addition the spectrum was not corrected for telluric lines which also cause minor deviation from the true EW when measured. Another reason was the non-refined line list used, which we have attempted to correct for here. The refined line list has made the derivation of the metallicity more reliable compared with the literature as it is demonstrated in Sec. 4.1. It is expected similar results will be obtained for this star once the final spectrum is presented, however the results should be more precise as it will not suffer for a bad wavelength calibration and telluric contamination.

All the above problems we had with HD 20010 have been solved for 10 Leo, and it is clear the results are of much higher quality. This can be seen by the smaller errors we have on our parameters, and the good agreement with all parameters compared with the literature. Therefore, it may be needed that a telluric correction is applied to the spectrum before atmospheric stellar parameters can be determined reliably. However, with our limited sample it is hard to make a clear conclusion yet.

6. Conclusion

After acquiring data for two early K giants (Arcturus and 10 Leo) we measured the EWs of a set of Fe I and Fe II lines. With these measurements and a second look at the solar spectrum, we refined the line list presented in Paper I. The EWs were manually measured for the Sun and the log gf values were calibrated afterwards. This allowed us to successfully determine parameters for the two early K giants, thus we are now making the bridge for the line list towards cooler temperatures. We revisited the F subgiant from Paper I (HD 20010) with the refined line list. Here we see an overall improvement compared to our previous results, confirming the refinement has worked. With the updated results for HD 20010, and the results for Arcturus and 10 Leo, we are now reaching the same precision as has been reached in the optical for similar spectral types using the same methodology. The obvious next step is the even cooler M stars. Particular interesting are the M dwarf stars, known to be prone forming rocky planets. As important as cooler stars, we have yet to test our line list on any dwarf stars other than the Sun for which our line list is calibrated. While it is expected that it will work for early K dwarf stars, it will still be an important accomplishment. The upcoming spectral library from CARMENES (priv. comm. with P. Amado) will feed the community with high quality spectra and allow us to extend our test to many different spectral types of interest.

Acknowledgements. We thank José Caballero for many useful for comments during the process which led to this paper. He has been most kind providing help whenever needed. This work was supported by Fundação para a Ciência e a Tecnologia, FCT, (ref. UID/FIS/04434/2013, PTDC/FIS-AST/1526/2014, and PTDC/FIS-AST/7073/2014) through national funds and by FEDER through COMPETE2020 (ref. POCI-01-0145-FEDER-007672, POCI-01-0145-FEDER-016886, and POCI-01-0145-FEDER-016880). N.C.S., and S.G.S. acknowledge the support from FCT through Investigador FCT contracts of reference IF/00169/2012, and IF/00028/2014, respectively, and POPH/FSE (EC) by FEDER funding through the program "Programa Operacional de Factores de Competitividade - COMPETE". E.D.M acknowledge the support from the FCT in the form of the grants SFRH/BPD/76606/2011. This research has made use of the SIMBAD database operated at CDS, Strasbourg (France).

References

Adibekyan, V. Z., Benamati, L., Santos, N. C., et al. 2015, MNRAS, 450, 1900
Aerts, C., Christensen-Dalsgaard, J., & Kurtz, D. W. 2010, Asteroseismology
Ammler-von Eiff, M., Santos, N. C., Sousa, S. G., et al. 2009, A&A, 507, 523
Andreasen, D. T., Sousa, S. G., Delgado Mena, E., et al. 2016, A&A, 585, A143
Andreasen, D. T., Sousa, S. G., Tsantaki, M., et al. 2017, A&A, 585, A143
Artigau, É., Kouach, D., Donati, J.-F., et al. 2014, in Society of Photo-Optical Instrumentation Engineers (SPIE) Conference Series, Vol. 9147, Society of Photo-Optical Instrumentation Engineers (SPIE) Conference Series, 15
Baraffe, I., Homeier, D., Allard, F., & Chabrier, G. 2015, A&A, 577, A42
Bensby, T., Feltzing, S., & Oey, M. S. 2014, A&A, 562, A71
Bertaux, J. L., Lallement, R., Ferron, S., Boonne, C., & Bodichon, R. 2014, A&A, 564, A46
Blackwell, D. E. & Shallis, M. J. 1977, MNRAS, 180, 177
Boyajian, T. S., von Braun, K., van Belle, G., et al. 2012, ApJ, 757, 112
Casagrande, L., Ramírez, I., Meléndez, J., Bessell, M., & Asplund, M. 2010, A&A, 512, A54
Conod, U., Blind, N., Wildi, F., & Pepe, F. 2016, in Proc. SPIE, Vol. 9909, Society of Photo-Optical Instrumentation Engineers (SPIE) Conference Series, 990941
da Silva, R., Milone, A. C., & Reddy, B. E. 2011, A&A, 526, A71
Delfosse, X., Donati, J.-F., Kouach, D., et al. 2013, in SF2A-2013: Proceedings of the Annual meeting of the French Society of Astronomy and Astrophysics, ed. L. Cambresy, F. Martins, E. Nuss, & A. Palacios, 497–508
Dotter, A., Chaboyer, B., Jevremović, D., et al. 2008, ApJS, 178, 89
Ducati, J. R. 2002, VizieR Online Data Catalog, 2237
Follert, R., Dorn, R. J., Oliva, E., et al. 2014, in Society of Photo-Optical Instrumentation Engineers (SPIE) Conference Series, Vol. 9147, Society of Photo-Optical Instrumentation Engineers (SPIE) Conference Series, 19

Gaia Collaboration, Prusti, T., de Bruijne, J. H. J., et al. 2016, A&A, 595, A1
Girardi, L., Bressan, A., Bertelli, G., & Chiosi, C. 2000, A&A Supp., 141, 371
Griffin, R. & Griffin, R. 1967, MNRAS, 137, 253
Hinkle, K., Wallace, L., Livingston, W., et al. 2003, in Cambridge Workshop on Cool Stars, Stellar Systems, and the Sun, Vol. 12, The Future of Cool-Star Astrophysics: 12th Cambridge Workshop on Cool Stars, Stellar Systems, and the Sun, ed. A. Brown, G. M. Harper, & T. R. Ayres, 851–856
Kjeldsen, H. & Bedding, T. R. 1995, A&A, 293, 87
Kotani, T., Tamura, M., Suto, H., et al. 2014, in Society of Photo-Optical Instrumentation Engineers (SPIE) Conference Series, Vol. 9147, Society of Photo-Optical Instrumentation Engineers (SPIE) Conference Series, 14
Kurucz, R. 1993, ATLAS9 Stellar Atmosphere Programs and 2 km/s grid. Kurucz CD-ROM No. 13. Cambridge, Mass.: Smithsonian Astrophysical Observatory, 1993., 13
Lebzelter, T., Heiter, U., Abia, C., et al. 2012, A&A, 547, A108
Lindgren, S., Heiter, U., & Seifahrt, A. 2016, A&A, 586, A100
Luck, R. E. 2015, AJ, 150, 88
Massarotti, A., Latham, D. W., Stefanik, R. P., & Fogel, J. 2008, AJ, 135, 209
McWilliam, A. 1990, ApJS, 74, 1075
Meléndez, J. & Barbuy, B. 1999, ApJS, 124, 527
Mortier, A., Santos, N. C., Sousa, S. G., et al. 2013, A&A, 558, A106
Mucciarelli, A., Pancino, E., Lovisi, L., Ferraro, F. R., & Lapenna, E. 2013, ApJ, 766, 78
Nicholls, C. P., Lebzelter, T., Smette, A., et al. 2016, ArXiv e-prints [e-prints[arXiv]1609.07873]
Önehag, A., Heiter, U., Gustafsson, B., et al. 2012, A&A, 542, A33
Origlia, L., Oliva, E., Baffa, C., et al. 2014, in Society of Photo-Optical Instrumentation Engineers (SPIE) Conference Series, Vol. 9147, Society of Photo-Optical Instrumentation Engineers (SPIE) Conference Series, 1
Park, S., Kang, W., Lee, J.-E., & Lee, S.-G. 2013, AJ, 146, 73
Quirrenbach, A., Amado, P. J., Caballero, J. A., et al. 2014, in Society of Photo-Optical Instrumentation Engineers (SPIE) Conference Series, Vol. 9147, Society of Photo-Optical Instrumentation Engineers (SPIE) Conference Series, 1
Ramírez, I., Allende Prieto, C., & Lambert, D. L. 2013, ApJ, 764, 78
Ramírez, I. & Meléndez, J. 2005, ApJ, 626, 446
Rayner, J., Bond, T., Bonnet, M., et al. 2012, in Proc. SPIE, Vol. 8446, Ground-based and Airborne Instrumentation for Astronomy IV, 84462C
Rayner, J., Tokunaga, A., Jaffe, D., et al. 2016, in Proc. SPIE, Vol. 9908, Society of Photo-Optical Instrumentation Engineers (SPIE) Conference Series, 990884
Recio-Blanco, A., Bijaoui, A., & de Laverny, P. 2006, MNRAS, 370, 141
Santos, N. C., Sousa, S. G., Mortier, A., et al. 2013, A&A, 556, A150
Soubiran, C., Bienaymé, O., Mishenina, T. V., & Kovtyukh, V. V. 2008, A&A, 480, 91
Sousa, S. G., Santos, N. C., Adibekyan, V., Delgado-Mena, E., & Israelian, G. 2015, A&A, 577, A67
Sousa, S. G., Santos, N. C., Mayor, M., et al. 2008, A&A, 487, 373
Torres, G., Fischer, D. A., Sozzetti, A., et al. 2012, ApJ, 757, 161
Torres, G., Winn, J. N., & Holman, M. J. 2008, ApJ, 677, 1324
Tsantaki, M., Sousa, S. G., Adibekyan, V. Z., et al. 2013, A&A, 555, A150
Valenti, J. A. & Fischer, D. A. 2005, ApJS, 159, 141

Appendix A: Complete refined line list

The complete refined line list with Solar EWs measured by hand using IRAF.

Table A.1. Refined line list with all Fe I and Fe II lines and corresponding atomic data, including the updated oscillator strengths.

Wavelength (Å)	Element	EP (eV)	log gf	Solar EW (mÅ)
10065.05	Fe I	4.83	-0.279	94.0
10080.42	Fe I	5.10	-1.964	5.9
10081.39	Fe I	2.42	-4.512	6.9
10086.24	Fe I	2.95	-3.978	7.0
10137.10	Fe I	5.09	-1.736	9.8
10142.84	Fe I	5.06	-1.554	14.9
10145.56	Fe I	4.80	-0.118	109.0
10155.16	Fe I	2.18	-4.336	16.2
10156.51	Fe I	4.59	-2.109	12.2
10167.47	Fe I	2.20	-2.319	125.7
10195.11	Fe I	2.73	-3.608	22.6
10216.31	Fe I	4.73	0.047	129.9
10218.41	Fe I	3.07	-2.893	40.9
10265.22	Fe I	2.22	-4.648	8.1
10307.45	Fe I	4.59	-2.432	6.4
10332.33	Fe I	3.63	-3.131	10.5
10340.89	Fe I	2.20	-3.665	46.6
10347.97	Fe I	5.39	-0.717	37.0
10353.81	Fe I	5.39	-0.989	24.2
10364.06	Fe I	5.45	-1.100	18.0
10379.00	Fe I	2.22	-4.236	18.7
10388.75	Fe I	5.45	-1.471	8.7
10395.80	Fe I	2.18	-3.435	61.3
10423.03	Fe I	2.69	-3.658	22.9
10423.74	Fe I	3.07	-3.119	29.9
10469.65	Fe I	3.88	-1.277	89.3
10532.24	Fe I	3.93	-1.650	64.4
10555.65	Fe I	5.45	-1.282	13.1
10577.14	Fe I	3.30	-3.222	17.2
10616.72	Fe I	3.27	-3.306	15.6
10725.19	Fe I	3.64	-2.948	15.7
10753.00	Fe I	3.96	-2.077	39.7
10780.69	Fe I	3.24	-3.553	10.4
10783.05	Fe I	3.11	-2.786	47.0
10818.28	Fe I	3.96	-2.160	35.6
10863.52	Fe I	4.73	-0.877	67.1
10884.26	Fe I	3.93	-2.129	39.1
10896.30	Fe I	3.07	-2.911	42.9
11013.24	Fe I	4.80	-1.240	42.4
11026.79	Fe I	3.94	-2.517	21.2
11119.80	Fe I	2.85	-2.452	84.8
11641.80	Fe I	4.58	-2.116	15.6
11778.42	Fe I	5.34	-1.708	8.4
12053.08	Fe I	4.56	-1.602	41.3
12119.50	Fe I	4.59	-1.897	25.0
12213.34	Fe I	4.64	-2.006	19.1
12227.11	Fe I	4.61	-1.408	51.5
12244.92	Fe I	3.64	-3.222	11.8
12340.48	Fe I	2.28	-4.680	9.4
12342.92	Fe I	4.64	-1.545	42.1
12510.52	Fe I	4.96	-1.930	12.9
12557.00	Fe I	2.28	-4.026	33.8
12615.93	Fe I	4.64	-1.686	35.7
12638.70	Fe I	4.56	-0.679	112.3
12807.15	Fe I	3.64	-2.649	37.1
12808.24	Fe I	4.99	-1.811	16.4
12824.86	Fe I	3.02	-3.612	20.1
12840.57	Fe I	4.96	-1.612	25.3
12879.77	Fe I	2.28	-3.525	68.7
12896.12	Fe I	4.91	-1.713	23.2

Table A.1. continued.

Wavelength (Å)	Element	EP (eV)	log gf	Solar EW (mÅ)
12933.01	Fe I	5.02	-1.879	13.9
12934.67	Fe I	5.39	-1.103	30.9
13014.84	Fe I	5.45	-1.542	12.3
13352.17	Fe I	5.31	-0.355	94.4
13392.10	Fe I	5.35	-0.105	115.1
15194.49	Fe I	2.22	-4.808	14.1
15201.57	Fe I	5.49	-1.315	29.0
15207.53	Fe I	5.38	0.311	215.9
15335.38	Fe I	5.41	0.252	205.2
15490.34	Fe I	2.20	-4.787	16.1
15593.74	Fe I	5.03	-1.796	28.0
15611.15	Fe I	3.42	-2.966	51.6
15631.95	Fe I	5.35	0.171	207.0
15648.51	Fe I	5.43	-0.633	93.8
15676.58	Fe I	5.11	-1.848	22.3
16198.50	Fe I	5.41	-0.376	131.4
17420.83	Fe I	3.88	-3.628	6.7
19923.34	Fe I	5.02	-1.536	49.7
21851.38	Fe I	3.64	-3.578	12.7
22257.11	Fe I	5.06	-0.704	132.5
22380.80	Fe I	5.03	-0.377	179.4
22392.88	Fe I	5.10	-1.330	60.8
22619.84	Fe I	4.99	-0.564	158.2
23308.48	Fe I	4.08	-2.705	31.3
10427.31	Fe II	6.08	-1.575	13.7
10501.50	Fe II	5.55	-1.861	19.5
10862.64	Fe II	5.59	-2.006	15.3
11125.58	Fe II	5.62	-2.213	10.5
13251.14	Fe II	9.41	0.768	13.4